Polarization-Independent Optical Switch with Multiple Sections of $\Delta\beta$ Reversal and a Gaussian Taper Function

O. G. RAMER, C. MOHR, AND J. PIKULSKI

Abstract—Multiple section $\Delta\beta$ reversal polarization-independent integrated optic switches have been designed and demonstrated at a 0.83 μm wavelength. These switches use a Gaussian taper function to achieve low crosstalk in the parallel state. Calculated switch characteristics as related to an ideal Gaussian taper and approximations that can be fabricated by mask making are described. Experimental demonstration shows that these switches have useful switching characteristics with relatively high switching voltages.

I. Introduction

THE filter characteristics of smoothly weighting or tapering the coupling between codirectional interacting waveguides and contradirectional Bragg reflection devices have been studied and reported [1]-[4]. Filters of both types have promise for use in integrated optical waveguide circuits for lightwave communications. Specific applications that have been identified are wavelength multiplexers or demultiplexers [5], polarization-independent optical switches or modulators [6], and Bragg mirrors [2].

An example of a codirectional filter is shown in Fig. 1. The interaction between the two modes in either device is described by a nonlinear Riccati equation [1], [3]. In general, the local coupling between the modes is described by a coupling coefficient $\kappa(z)$. Several functional relations for $\kappa(z)$ have been studied for their filter characteristics. The ones producing the lowest sidelobe levels to date have been a set of "window" functions that have been thoroughly studied for their properties as digital filters [3]. In this paper, we consider a truncated Gaussian to describe the functional behavior of $\kappa(z)$.

Of primary consideration in this paper is the design and demonstration of a codirectional polarization-independent switch using the Gaussian taper function and multiple sections of $\Delta\beta$ reversal at a wavelength λ of 0.83 μm. This work follows that of Alferness [6] who worked at a $\lambda = 0.63$ μm and used a single section $\Delta\beta$ reversal and the Hamming taper function. Fortunately, $LiNbO_3$ does not suffer from the extreme optical damage at $\lambda = 0.83$ μm that exists at $\lambda = 0.63$ μm, which makes the switch described here potentially useful in optical systems.

Manuscript received March 1, 1982; revised May 18, 1982. This work was supported by the Naval Research Laboratory under Contract N00173-80-C-0439.

The authors are with the Hughes Research Laboratories, Malibu, CA 90265.

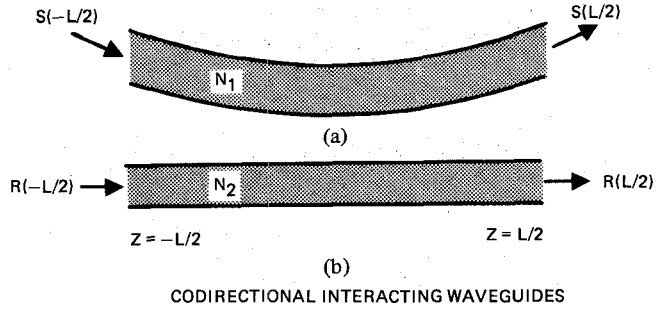

Fig. 1. Schematic diagram of coupled optical modes.

The polarization-independent switch was fabricated with Ti-diffused waveguides on Z-cut $LiNbO_3$. It consists of a directional coupler (Fig. 2), with the coupling coefficient κ carefully weighted (with a truncated Gaussian taper function) along the length by varying the interguide separation d. Split electrodes are used to allow application of either the reversed $\Delta\beta$ or the uniform $\Delta\beta$ field configuration.

As in a single polarization switch, the crossover state, where light incident in one guide emerges in the other guide, is obtained by imposing field polarity changes on the guides, producing the well-known $\Delta\beta$ reversal switch; field polarity changes are obtained by placing equal and opposite voltages on adjacent electrodes. To obtain a good cross state, the operational conditions require that for both polarizations, the integral of the coupling coefficient over the length of the device be nearly $\sigma\pi/2$ (σ = 1, 3, 5, etc.). This corresponds to the waveguide device being in an approximate cross state. This constraint is primarily associated with the effect of the applied electric field on the two polarizations. For a Z-cut crystal orientation and the electrode placement illustrated in Fig. 2 and for single-mode waveguides, $\Delta\beta_{TM}/\Delta\beta_{TE} \approx 2.67$. The integrated coupling strengths for the TE and TM modes can be made equal for Z-cut $LiNbO_3$ by an appropriate choice of waveguide and coupler parameters.

The straight-through state is obtained by applying the same voltages to all electrodes, thereby creating a uniform phase mismatch along the tapered coupler. The straight-through state can be obtained even with large differences in the electro-optic effect filter characteristic of the tapered directional coupler.

Section II describes the theoretical filter characteristics obtained when the truncated Gaussian is used as the taper

0018-9480/82/1000-1760$00.75

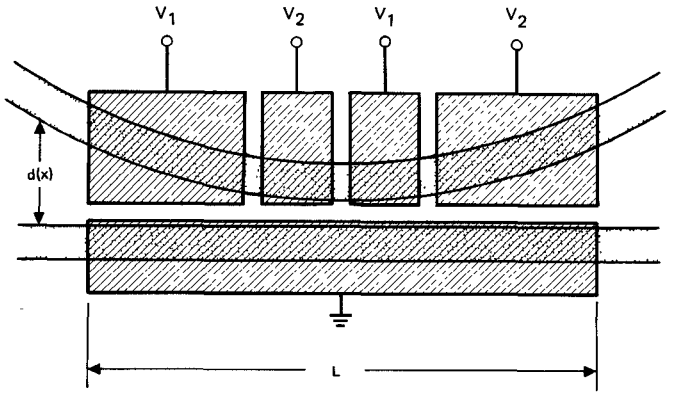

Fig. 2. Diagram of $\Delta\beta$ reversal polarization-independent switch.

function. Section III describes the experimental characterization of the coupling coefficient required for switch design. Section IV describes the design of a multisection $\Delta\beta$ reversal polarization-independent optical switch utilizing the Gaussian taper function. Section V describes the experimental demonstration of the designed device.

II. Gaussian Taper Function

The function investigated in this study has been truncated Gaussian function

$$w(z) = \frac{2\alpha}{\sqrt{\pi}} e^{-(2\alpha z/L)^2} \Big/ \operatorname{erf}(\alpha) \tag{1}$$

where

$$\kappa(z) = sw(z)/L \tag{2}$$

$$\int_{-L/2}^{L/2} w(z)\, dz = L \tag{3}$$

and the integrated coupling strength is s. As was the "window" function [3], the truncated Gaussian has been utilized because of the very low Fourier transform sidelobe that can be achieved. For the nontruncated Gaussian ($\alpha = \infty$), the Fourier transform is another Gaussian which does not contain sidelobes. For the truncated Gaussian, the value of α can be used as a variable in obtaining the desired sidelobe level and in optimizing the filter response. The calculated [1], [3] filter responses for a codirectional coupler with $s = \pi/2$, $3\pi/2$, and $5\pi/2$ are shown in Fig. 3. The parameter in each figure is the truncation factor α.

In order to fabricate the polarization-independent switch, it is necessary to design a mask that will result in waveguides having the desired variation of $\kappa(z)$. This design is constrained by the mask or pattern generator, and will result in an approximate Gaussian variation of $\kappa(z)$, assuming that the exact dependence of κ versus the waveguide separation is known. Typically, pattern generators have 0.1° angular resolution and 0.1 and 0.5 μm displacement resolution. With these constraints, two possible "fits" to the Gaussian are tangential segments at 0.1° angular increments, and parallel (0°) segments displaced by an amount equal to the resolution of the pattern generator. The former fit produces the minimum number of discrete discontinuities in the waveguide. Effects on the filter characteristics due to fitting [3] will be shown after the design details of the PIOS are discussed in Section III. Some mathematical expressions characteristic of the Gaussian taper useful in mask design are derived below.

There is no analytical description for the modal field of a single mode diffused channel waveguide or for the coupling coefficient κ for codirectional couplers. However, the coupling between two $LiNbO_3$ Ti-diffused guides has been shown experimentally to be given by

$$\kappa = \kappa_0 e^{-d/\gamma} \tag{4}$$

where κ_0 and γ depend on waveguide parameters, but are independent of d, the separation between guides [7], [8]. Therefore, given κ_0, γ, α, s, and L, $d(z)$ is given by a single quadratic equation:

$$d(z) = -\gamma \ln \frac{2s\alpha}{L\kappa_0\sqrt{\pi}\operatorname{erf}(\alpha)} + \gamma(2\alpha/L)^2. \tag{5}$$

In order to fit the taper with angular incremented segments, one has to determine the tangential points. For the Gaussian dependence of $\kappa(z)$, the position where the taper function has a slope $m = dd/dz$ is

$$z(m) = L^2 m/8\gamma\alpha^2. \tag{6}$$

Finally, in order to fit the curve with incremental steps or parallel segments, one has to determine the position $z(d)$ where the incremental steps occur:

$$z(d) = \frac{\pm L}{2\alpha}\sqrt{\frac{d}{\gamma} + \ln\left(\frac{2\alpha s}{\sqrt{\pi}\operatorname{erf}(\alpha) L\kappa_0}\right)}. \tag{7}$$

III. Experimental Coupler Characterization

Before one can carry out a switch design, it is necessary to know the parameters γ and κ_0 in (4). The method for determining this functional dependence is to experimentally determine κ for several waveguide separations and fit the data to obtain κ_0 and γ.

During this program, a number of samples for characterization of the transfer length were generated. A large range of Ti concentrations and gas flow conditions were covered. In all cases, the intersection of the TE and TM l versus d curves (Fig. 4) resulted in a very short device ($L < 1$ mm) which was not appropriate for the successful fabrication of a $\pi/2$ switch. (The required switch voltage would have been excessive.) The approach taken to reduce the switch voltage was to increase the device length by using a multiple $\Delta\beta$ reversal design for the cross state.

IV. Polarization-Independent Optical Switch (PIOS) Design

In general, the coupling coefficients for the two polarizations of $LiNbO_3$:Ti-diffused waveguides are unequal. At a narrow waveguide separation, the coupling coefficient for the TE polarization is typically larger than that for the TM polarization. The reverse is typically true for wider waveguide separations. This situation makes it possible to design a tapered waveguide system so that

$$\int_{-L/2}^{L/2} \kappa_{TE}\, dz = \int_{-L/2}^{L/2} \kappa_{TM}\, dz = s \tag{8}$$

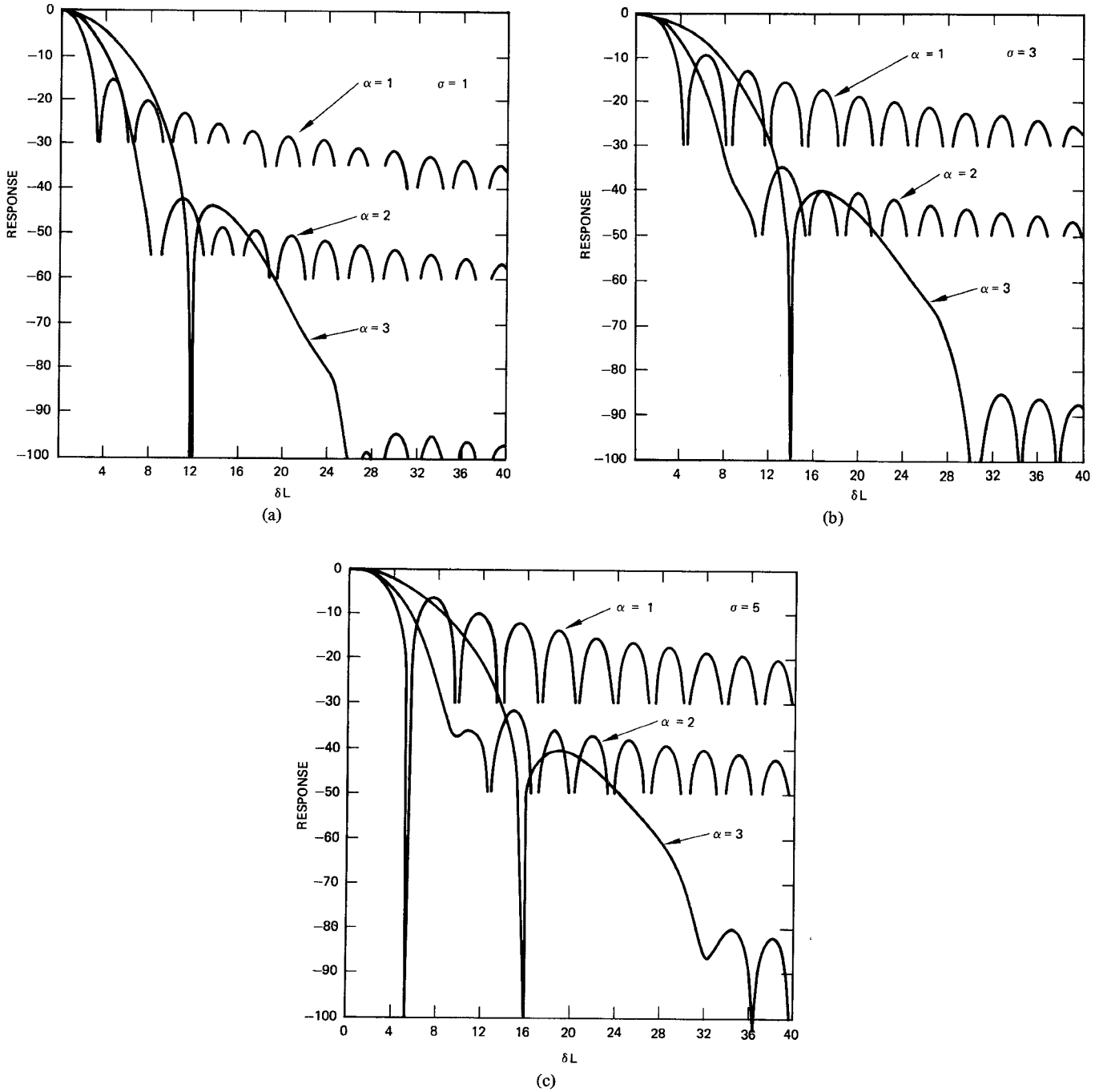

Fig. 3. Truncated Gaussian taper codirectional filter responses with $\alpha = 1, 2$, and 3. (a) $\sigma = 1$. (b) $\sigma = 3$. (c) $\sigma = 5$.

by digitally determining the appropriate length L of the device. This capability is basically the requirement to achieve a cross state in the polarization-independent optical switch considered in this paper. The parallel state is obtained by relying on the filter response of the device.

As pointed out by Alferness [6], the requirements for the PIOS design include, for the cross state,

$$s \approx \sigma\pi/2 \qquad \sigma = (1, 3, 5, \cdots) \tag{9}$$

and for the parallel state, the taper function $w(z)$ is considered to be a function having low Fourier transform sidelobes. In our design, the taper function utilized is the truncated Gaussian discussed earlier. The switch demonstrated by Alferness had a $\sigma \simeq 1$. The remainder of this section deals with the design characteristics of switches with $\sigma > 1$ which have not previously been described in the literature. Variations from the $\sigma = 1, 3, 5 \cdots$ condition in the device can be adjusted by the $\Delta\beta$ reversal electrode in a fashion similar to that explained by Alferness.

For a truncated Gaussian function, the value of α can be

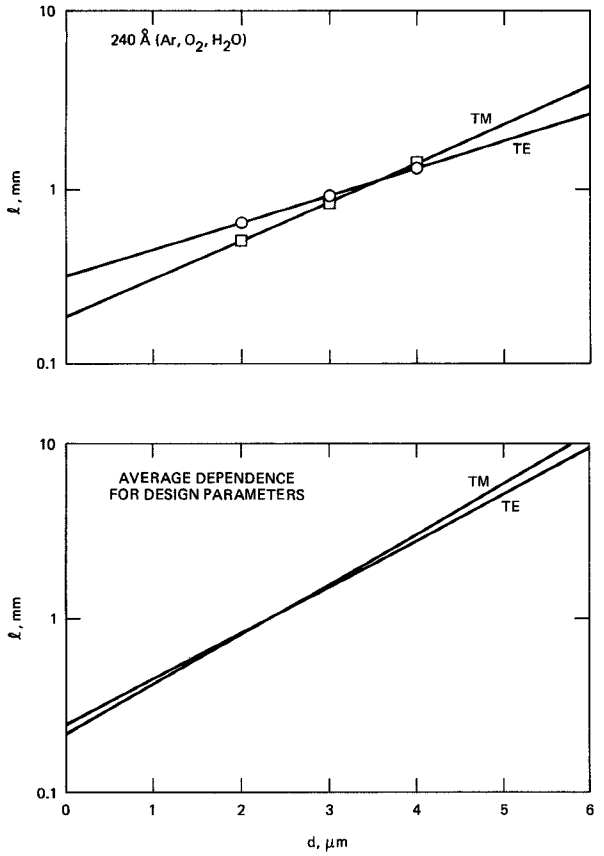

Fig. 4. Example l versus d behaviors for several samples $l = \pi/2\kappa$.

used as a variable in optimizing the filter response. Some of the factors involved in the selection of α are plotted in Fig. 5. These data were generated using experimentally determined values of γ and κ_0 (Table I); the waveguides were fabricated on Z-cut $LiNbO_3$ using 360 Å Ti and 1000°C, 8 h diffusion; the Li_2O out-diffusion mode was eliminated by using a water bubbler, and by flowing Ar during diffusion and flowing O_2 during cool down.

The interaction length L is plotted in Fig. 5(a). More important, however, is the value of δ at −20 dB optical crosstalk (the design goal for the switch), which is proportional to the required switch voltage [Fig. 5(b)]. The minimum and maximum [Fig. 5(c)] guide separation are important dimensions in the PIOS design; the coupling length versus guide separation is plotted in Fig. 4. In general, the smaller the α, the lower the switch voltage; however, α must be large enough so that at $d_{\max}$, the guides approximate the condition $\kappa(d_{\max}) = 0$.

The other necessary selection in the design of a PIOS is σ [see (9)]. Increasing σ increases the device length; in fact, $L_\sigma = \sigma L_1$. The longer the device, the lower the required switch voltage, but the voltage does not drop as (σ^{-1}). Plotted in Fig. 3 is the filter response for $\sigma = 1, 3, 5$ (in the associated calculations, $L_\sigma = \sigma L_1$). The associated δ's for −20 dB crosstalk for the TE polarization versus the value of α, with σ as a parameter, is plotted in Fig. 5(b) ($\Delta\beta_{TM} = 2.67 \times \Delta\beta_{TE}$ for Z-cut $LiNbO_3$ at 0.83 μm wavelength). It is apparent that for higher σ's, the switch voltage is reduced, i.e., reduced δ. The final consideration in the selection of σ is the response after fitting the truncated Gaussian to what can be achieved by mask masking. Plotted in Fig. 6 for $\alpha = 2$ are the filter responses for $\sigma = 1$, 3, and 5 using 0.1° angularity incremented segments to approximate the taper function. The ideal responses are given in Fig. 3. The very obvious degradation at $\sigma = 3$ and 5 is associated with the accuracy to which the angular segments can approximate the taper function. As σ increases, the number of segments decreases on the same order as $1/\sigma$ since the length of interaction increases on the same order as $L = \sigma L_1$, but $d_{\min}$ and $d_{\max}$ remain constant.

If values of $\sigma > 3$ are required (for example, to reduce the switch voltage), one has to consider fabricating the mask using parallel segments displaced by an amount equal to the resolution of the pattern generator. Thus, for 0.1 μm displacements between segments and $\alpha = 2$, the filter response for $\sigma = 5$ is plotted in Fig. 7. For this technique, the number of parallel segments remains constant as σ increases; however, the segment length is proportional to σ. The primary disadvantage of this approach is the large number of discrete waveguide discontinuities and mask fabrication complexity.

The switch waveguide was designed with the mask digitization, fabrication capabilities, and device loss in mind. Due to the lower potential optical loss of the tangential segments, our design utilized this fit to the Gaussian taper function; the angular increment was 0.1°. In addition, Gaussian taper values of $\alpha = 2$ and $\sigma = 3$ were chosen. Fig. 6 shows the calculated filter response for this segmented taper function.

Another advantage of the multiple section $\Delta\beta$ reversal polarization-independent switch over the two-section switch around $\sigma = 1$ is an extension of the waveguide fabrication tolerance by versatile electrode design. For example, assuming that $\sigma \cong 5$ and $\sigma > 5$, then a six-section electrode can be used. However, if $\sigma < 5$, then a four-section electrode is required to achieve the minimum crosstalk cross state (see Fig. 8).

The lengths of the $\Delta\beta$ reversal segments are not equal, as in the nontapered switch, due to the variation of κ with z. The length of the segments is determined by the requirement

$$\int w\, dt = \frac{L}{N} \tag{10}$$

where the integral is over the length of the segment and N is the number of segments desired. For the left outside segment of the four-section switch,

$$\int_{-L/2}^{Z} w\, dt = \frac{L}{2\,\mathrm{erf}\,(\alpha)}\left[\mathrm{erf}\,(\alpha) - \mathrm{erf}\left(\frac{2\alpha Z}{L}\right)\right] = L/4 \tag{11}$$

or

$$\frac{\mathrm{erf}\,(\alpha)}{2} = \mathrm{erf}\left(\frac{2\alpha Z}{L}\right). \tag{12}$$

By approximating erf $(\alpha) \cong 1$ (erf (2) = 0.99532 · · ·), we have

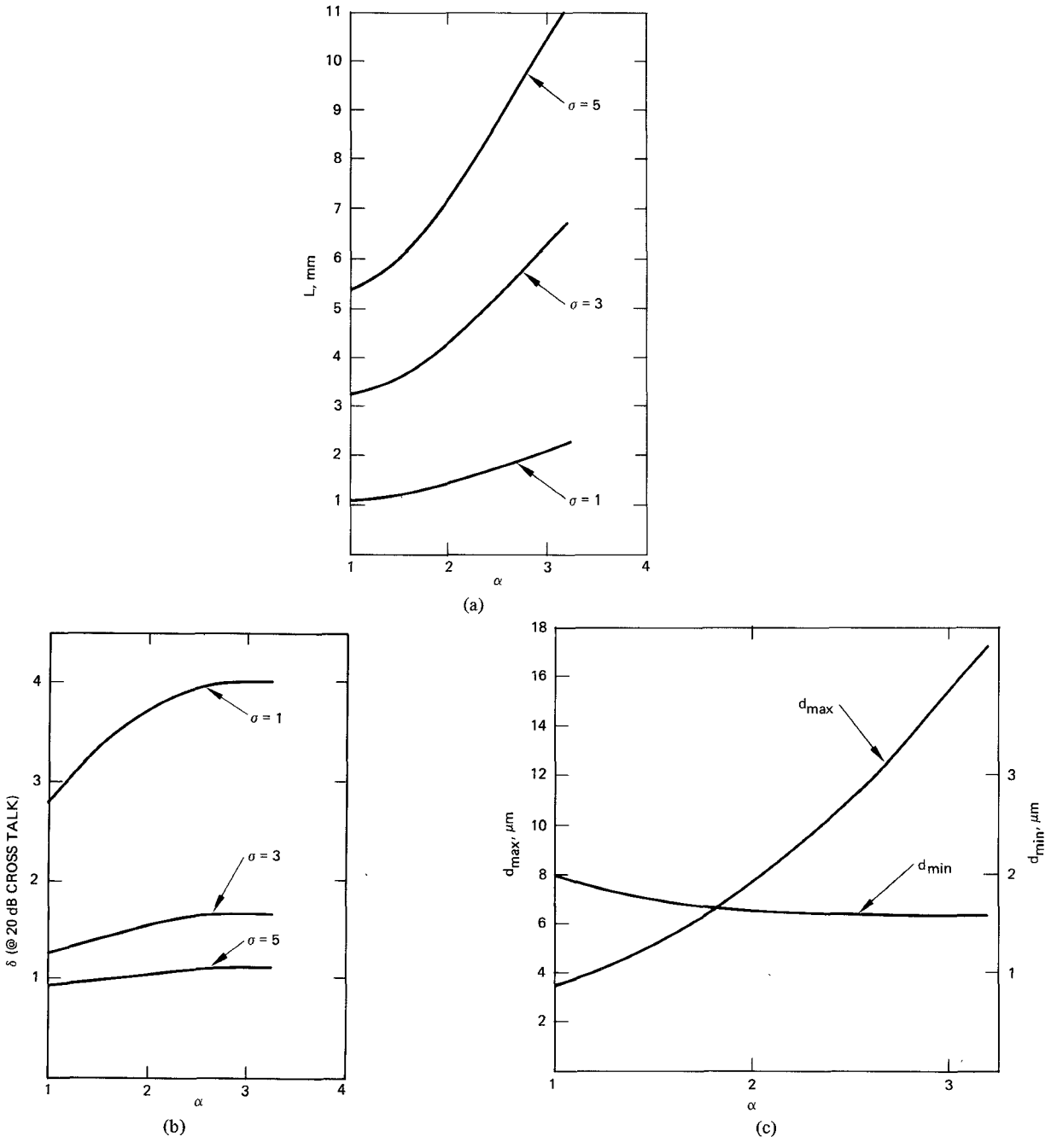

Fig. 5. Design characteristics of the truncated Gaussian polarization-independent switch.

$$Z = \frac{0.238L}{\alpha}. \tag{13}$$

A photograph of the four-section electrode fabricated for this program is shown in Fig. 9. The electrode was designed assuming $\sigma > 3$; in the event that $\sigma < 3$ in the waveguide device, the electrode can be easily modified to allow two-section reversal switch operation.

V. Experimental Demonstration

This section discusses the experimental demonstration of the four-section $\Delta\beta$ reversal polarization-independent switch at 0.83 μm. The switch was fabricated on Z-cut $LiNbO_3$ using 4 μm wide stripes of 360 Å thick Ti diffused 8 h at 1000°C in the presence of Ar passed through a water bubbler; during cool down, the Ar was replaced with O_2. A 2500 Å SiO_2 buffer layer was sputter-deposited on the $LiNbO_3$ before fabrication of the electrodes. The SiO_2 was used to eliminate the optical loss associated with the metal optical mode interactions. The spacing between the waveguides in the interaction region varied approximately quadratically (5), corresponding to a Gaussian variation in the coupling coefficient (1)-(3); γ, κ_0 are given in Table I; $\alpha = 2$ and $\sigma = 3$. The approximation is due to mask-making capabilities discussed in Sections III and IV. The interaction region is 4.57 mm in length, the maximum interaction region guide separation is 7.8 μm, and the minimum guide spacing is 1.77 μm. Outside

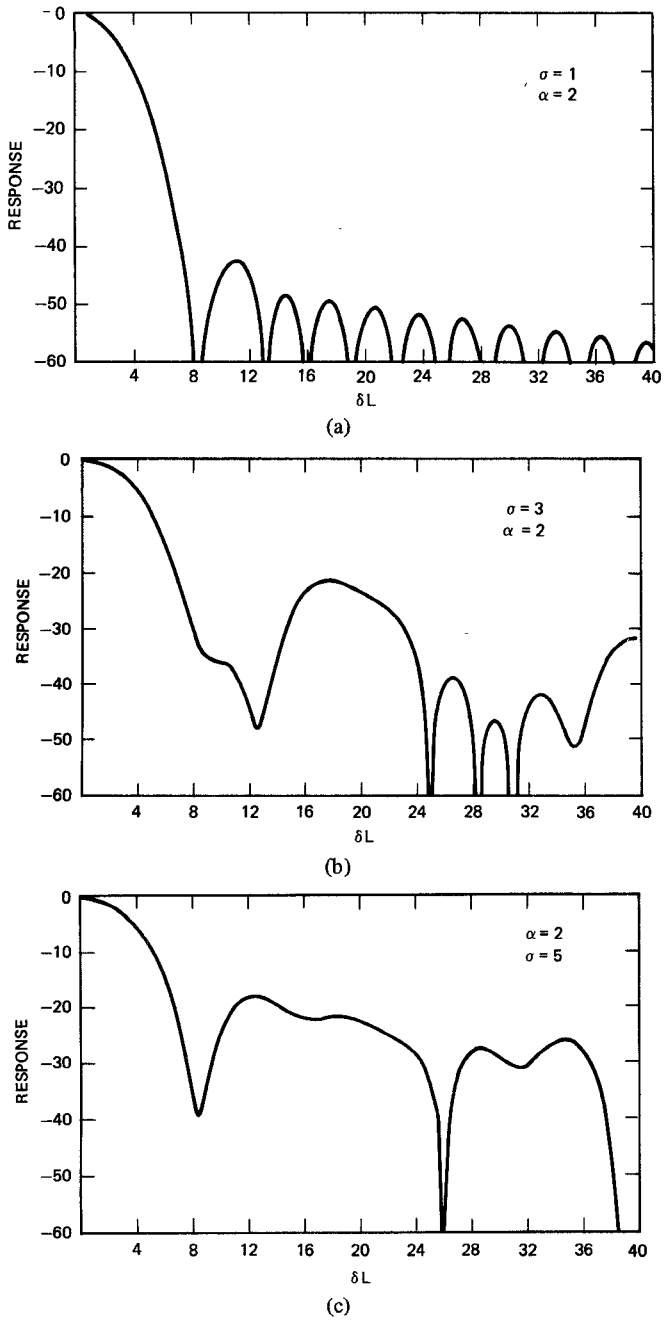

Fig. 6. Approximated Gaussian taper ($\alpha = 2$) filter responses where tangential segments are used. (a) $\sigma = 1$. (b) $\sigma = 3$. (c) $\sigma = 5$.

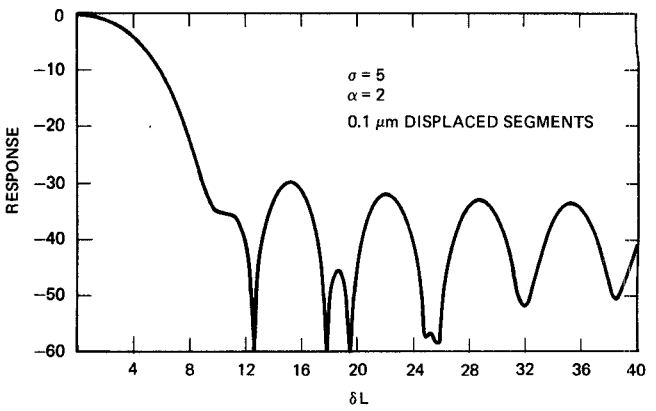

Fig. 7. Approximated Gaussian taper ($\sigma = 2$, $\sigma = 5$) filter response where parallel misplaced segments are used.

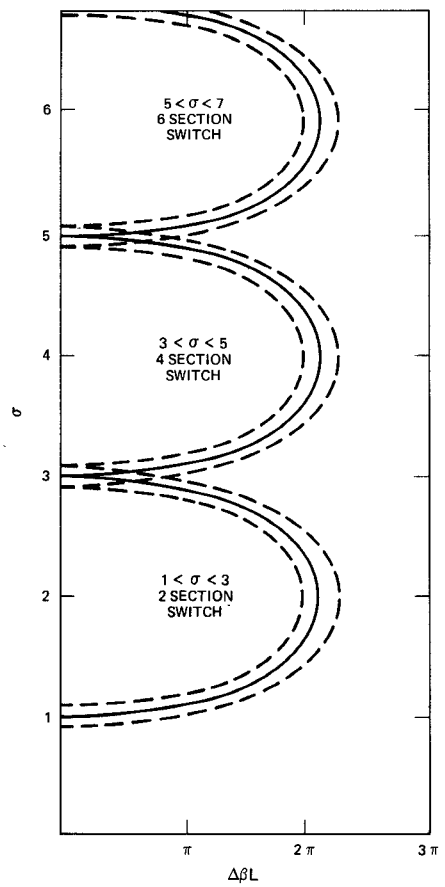

Fig. 8. Representation of −20 dB crosstalk limits for different values of σ and number of $\Delta\beta$ reversal sections.

the interaction region, the guides separate to 130 μm at a relative slope of 2°. The device is shown schematically in Fig. 2, which is followed in Fig. 9 by an actual photograph.

The tests were conducted using an optical end fire test setup. The laser diode was mounted with polarization oriented 45° with respect to the $LiNbO_3$ Z axis; this gives equal TE and TM excitation at the input face of the device. A polarizer can be placed before the chip to select either the TE or TM mode for individual polarization operation. The source of electrical power was a center-tapped variac connected to the 110 V ac outlet. This provided 60 Hz signals of equal and opposite polarity with respect to ground. Measurements were not conducted at dc due to the drift associated with the presence of the SiO_2 buffer layer. Relative optical intensities were measured using an APD with a 50 Ω load connected to an oscilloscope. Data were recorded by taking photographs of the oscilloscope output. Shown in these photogrpahs are the drive signal and detected optical output.

The first series of photographs (Fig. 10) was taken with the electrical configuration corresponding to a constant (i.e., non-$\Delta\beta$ reversal) polarity electric field across the whole interaction region. In this configuration, the parallel state operation of the switch is demonstrated. The relationship of the optical input and output ports associated with the the photographs is illustrated in the figures. The polarization of the

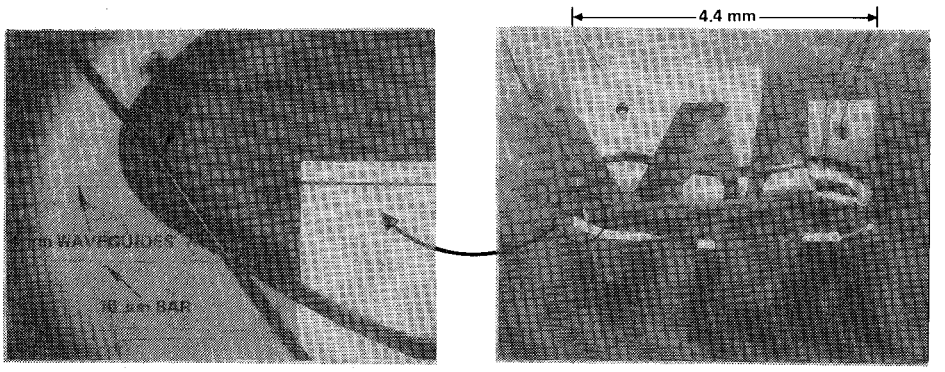

Fig. 9. Photograph of polarization-independent switch.

TABLE I
DESIGN WAVEGUIDE PARAMETERS

Mode Parameters	κ_o μm^{-1}	γ μm^{-1}
TE	6.44	1.64
TM	7.22	1.52

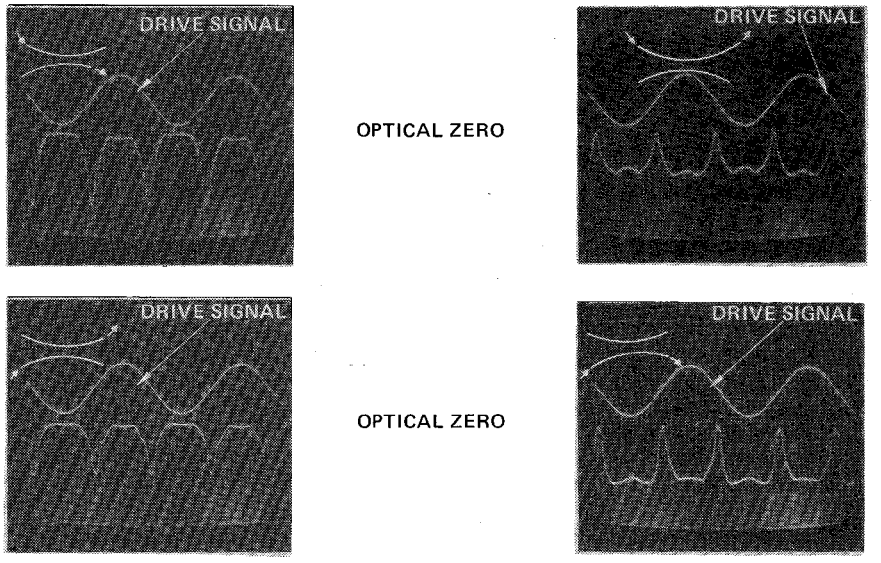

Fig. 10. Constant polarity electric field test result wih both TE and TM polarizations excited.

input signals is 45° with respect to the crystal Z axis. The drive signal is displayed at 100 V/div; zero voltage is clearly marked by the crossover distortion. These photographs clearly point out the following characteristics of the device.

1) The device is near a cross state with zero applied voltage (crosstalk ~ −12 dB).

2) The device is not perfectly symmetrical with respect to zero applied signal. The amount of asymmetry is device-dependent, and is believed to be due to processing defects.

3) The device requires a drive signal larger than 100 V to achieve excellent parallel state crosstalk. The device has had as much as 150 V applied without electrode breakdown. At this increased voltage, better than 20 dB crosstalk levels were observed.

The filter function behavior of both polarizations is illustrated in Fig. 11. These data were obtained by placing a polarizer between the laser and the chip. The data show that the majority of the crosstalk at 100 V is due to the TE polarization, and that increased applied voltage is required to reach the first null in the response.

The next series of photographs (Fig. 12) was taken with the electrical configuration corresponding to the $\Delta\beta$ reversal electrode. In this configuration, the cross-state operation of the switch is demonstrated at a 0.83 μm wavelength. Using the crossover distortion as a zero voltage reference, improved cross-state performance is demonstrated with only a few volts; the drive signal is displayed at 10 V/div. The asymmetry of the device is, however, very apparent. With one polarity, the

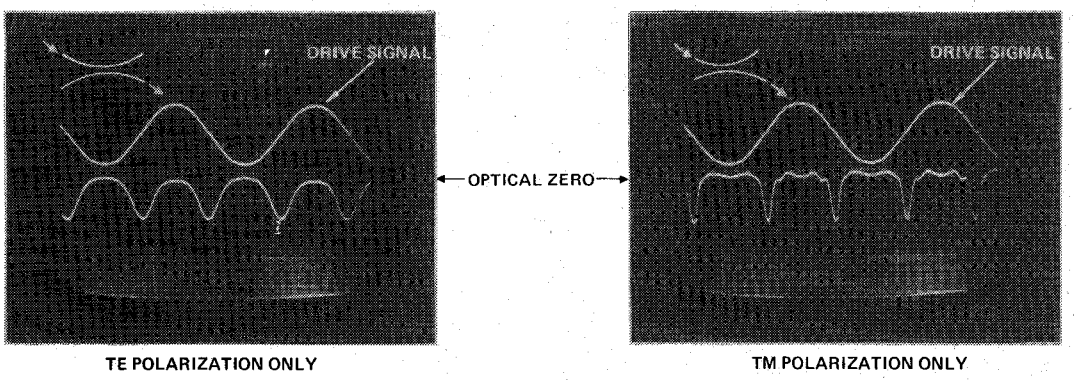

Fig. 11. Individual polarization operation with constant polarity electric field.

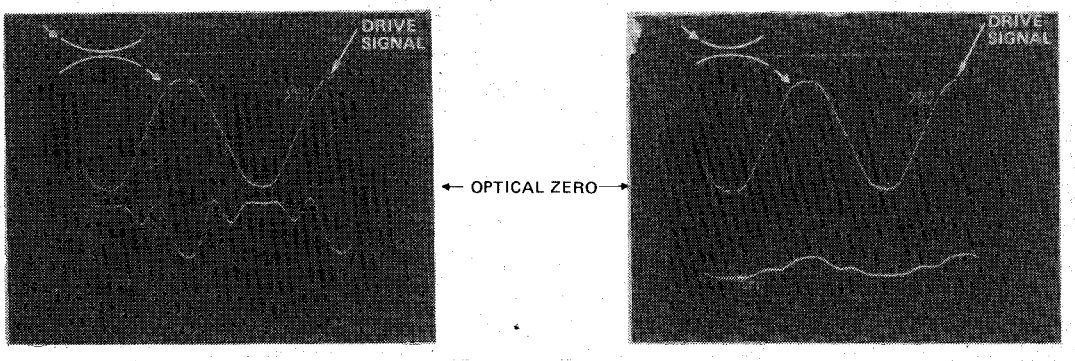

Fig. 12. $\Delta\beta$ reversal test results showing the cross state. Both polarizations were excited.

minimum crosstalk occurs with ~20 V. The crosstalk level achieved in Fig. 12 is ~16 dB. This can be enhanced by appropriate variation of the processing parameters.

VI. Discussion

This program has resulted in the demonstration of a polarization-independent switchable directional coupler. Noteworthy accomplishments include the design and fabrication of a four-section $\Delta\beta$ reversal polarization-independent switch at a 0.83 μm wavelength, and the theoretical and experimental investigation of the filter characteristics of a Gaussian taper function. Based on this extensive work, it is apparent that additional research needs to be conducted in the areas of device design and fabrication in order to reduce switch voltage, waveguide losses, polarization noise, and to allow dc switch operation.

Acknowledgment

The authors would like to thank R. V. Schmidt for his many useful discussions.

References

[1] H. Kogelnik, "Filter response of non-uniform almost-periodic structure," *Bell Syst. Tech. J.*, vol. 55, p. 109, 1976.
[2] P. S. Cross and H. Kogelnik, "Sidelobe suppression in corrugated-waveguide filters," *Opt. Lett.*, vol. 1, p. 43, 1977.
[3] R. C. Alferness and P. S. Cross, "Filter characteristics of codirectionally coupled waveguides with weighted coupling," *IEEE J. Quantum Electron.*, vol. QE-14, p. 843, 1978.
[4] R. C. Alferness, "Optical directional couplers with weighted coupling," *Appl. Phys. Lett.*, vol. 35, p. 260, 1979.
[5] R. C. Alferness and R. V. Schmidt, "Tunable optical waveguide directional coupler filter," presented at the Topical Meet., Integrated and Guided Wave Opt., June 1978; also in *Appl. Phys. Lett.*, vol. 33, pp. 161-163, 1978.
[6] R. C. Alferness, "Polarization-independent optical directional coupler switch using weighted coupling," *Appl. Phys. Lett.*, vol. 35, p. 748, 1979.
[7] E.A.J. Marcalili, "Dielectric rectangular waveguide and directional coupler for integrated optics," *Bell. Syst. Tech. J.*, vol. 49, pp. 2071-2102, Sept. 1969.
[8] R. C. Alferness, R. V. Schmidt, and E. H. Turner, "Characteristics of Ti-diffused lithium niobate optical directional couplers," *Appl. Opt.*, vol. 18, p. 4012, 1979.

O. G. Ramer, for a photograph and biography, see p. 392 of the March 1982 issue of the Journal of Quantum Electronics.

C. Mohr, photograph and biography not available at the time of publication.

J. Pikulski, photograph and biography not available at the time of publication.